Sustainable Food Technology

ROYAL SOCIETY OF CHEMISTRY

PAPER

View Article Online
View Journal | View Issue

Cite this: *Sustainable Food Technol.*, 2023, **1**, 941

Acid-derived bacterial cellulose nanocrystals as organic filler for the generation of high-oxygen barrier bio-nanocomposite coatings†

Daniele Carullo,‡[a] Cesare Rovera, ‡[a] Tommaso Bellesia,[a] Duygu Büyüktaş,[ab] Masoud Ghaani,[ac] Nadia Santo,[d] Diego Romano[a] and Stefano Farris *[a]

Macro-sized bacterial cellulose (BC) derived from *Komagataeibacter sucrofermentans* was down-sized into nanocrystals (BCNCs) through hydrochloric acid (H-BCNCs) and sulfuric acid (S-BCNCs) hydrolysis. Initially, aqueous dispersions of BCNCs were analyzed for stability, size/morphology, and optical/mechanical properties. Subsequently, BCNCs were incorporated into a main biopolymer phase (*i.e.*, pullulan) to create bio-nanocomposite coatings with high-oxygen barrier performance. Upon treatment with sulfuric acid, nano-sized particles (≈240 nm) were observed, contrasting with significantly larger sizes (≈1.8 μm) seen for particles obtained using hydrochloric acid. Microscopy analyses revealed a needle-like morphology of the nanocrystals, which appeared organized in stacks for H-BCNCs or as individual units for S-BCNCs. Pullulan/BCNCs coatings applied to polyethylene-terephthalate (PET) films improved the gas barrier performance of the original substrate, by dramatically reducing the oxygen transmission rate (OTR) values from ≈ 120 cm^3 m^{-2} 24 h^{-1} to ≈ 2 cm^3 m^{-2} 24 h^{-1} while preserving its original optical and mechanical properties. Our developed bionanocomposite-coated PET films hold potential as an alternative material for various food packaging applications.

Received 26th August 2023
Accepted 18th October 2023

DOI: 10.1039/d3fb00147d

rsc.li/susfoodtech

Sustainability spotlight

While dominated by materials of non-renewable origin, the food packaging sector is on the verge of an extraordinary revolution towards safer and more sustainable solutions. In an attempt to achieve a more profitable use of natural sources, new strategies and approaches are highly sought. Cellulose and its derivatives have the potential to create new packaging films and coatings with enhanced performance. In this regard, cellulose nanocrystals can be advantageously used as nanobuilding blocks for the generation of bionanocomposite materials when incorporated into a primary biopolymer phase, thus allowing the replacement of conventional fossil-based systems. This study emphasizes the importance of UN sustainability development goals (SDG 2023): zero hunger (SDG 2), industry, innovation and infrastructure (SDG 9), and responsible consumption and production (SGD 12).

1. Introduction

In recent years, there has been a growing interest in developing new packaging configurations using materials of renewable origin.[1] Natural nanofibers, in particular, have been investigated as a potential alternative to synthetic food packaging materials.[2] Among these, cellulose and its derivatives have garnered significant attention. This interest stems not only from their inherent biodegradability but also from their wide availability. Notably, the extraction of cellulose from sources beyond wood has been demonstrated, such as agri-food waste and residues,[3–5] and even bacteria.[6,7]

Bacterial cellulose (BC) is synthesized in high yield by Gram-negative acetic acid bacteria, primarily belonging to families like *Komagataeibacter xylinus*, *Gluconacetobacter hansenii*, *Acetobacter pasteurianus*, and *Komagataeibacter sucrofermentans*.[8] The prominent feature of BC is its high purity, devoid of collateral biogenic compounds like lignin, hemicelluloses, organic compounds, and pectin found in plant cellulose.[9] This characteristic profoundly influences the assembly pattern of cellulose chains, resulting in the formation of crystal units—highly ordered domains where glucan chain sheets align and stack.[10] This organization ultimately leads to a greater degree of crystallinity in native BC's alpha-cellulose (Iα), ranging from 84% to 89%, compared to the beta-cellulose (Iβ) in plant-

[a]*DeFENS, Department of Food, Environmental and Nutritional Sciences, University of Milan, via Celoria 2, I-20133 Milan, Italy. E-mail: stefano.farris@unimi.it*

[b]*Department of Food Engineering, Faculty of Engineering, Izmir Institute of Technology, 35430, Gülbahçe Köyü, Urla, Izmir, Turkey*

[c]*Department of Civil, Structural & Environmental Engineering, School of Engineering, Trinity College Dublin, Dublin, Ireland*

[d]*UNITECH NOLIMITS – NOvel Live bioImaging Milano cItTà Studi centre, University of Milan, via C. Golgi 19, I-20133 Milan, Italy*

† Electronic supplementary information (ESI) available. See DOI: https://doi.org/10.1039/d3fb00147d

‡ These authors contributed equally to this work.

derived counterparts (40% to 60%).[11,12] This high crystallinity is crucial for the development of nanocomposite materials due to its substantial impact on functional properties like mechanical, thermal, and barrier properties.[13,14]

To this end, the isolation of crystalline domains from BC's amorphous phase to obtain bacterial cellulose nanocrystals (BCNCs) has paved the way for high-performance nanocomposite materials. BCNCs serve as an alternative to conventional inorganic nanobuilding blocks (NBBs)[8,15] for the creation of bionanocomposites that can replace conventional, non-biodegradable petroleum-based plastic packaging materials.[16] BCNCs have been successfully obtained through chemical,[17] physical,[18] and enzymatic[8] routes or their combinations. While physical and enzymatic approaches are environmentally friendly, certain drawbacks limit their potential compared to chemical methods—such as low process efficiency and broad polydispersity of the BCNCs obtained.

Among the methods, acid hydrolysis stands as the most widely used approach for obtaining high-quality nanocrystals from cellulosic sources. Acid selectively attacks the amorphous domains of the cellulose backbone, yielding rod-like nanocrystals in significant quantities.[17] Sulfuric and hydrochloric acids have been extensively used to produce cellulose nanocrystals, each impacting the final product differently. Notably, Arserim-Uçar *et al.* (2021)[19] highlighted that using distinct hydrolytic conditions (temperature and acid type) for producing BCNCs using sulfuric and hydrochloric acids results in varying outputs regarding size distribution and crystallinity index without affecting thermal stability.

In the realm of food packaging, cellulose nanocrystals have proven successful as organic nanofillers incorporated into various polymer phases as reinforcing agents, even at concentrations as low as 1 wt%.[20] Cellulose nanocrystals have enhanced tensile strength and thermal stability of biopolymers like polylactic acid (PLA)[21–23] and polybutylene-succinate (PBS).[24,25] Additionally, they have provided benefits such as UV shielding, antimicrobial activity, and improved gas barrier properties in the final nanocomposite materials.[26,27]

However, the use of cellulose nanocrystals as organic fillers incorporated into (bio)polymer layers coated on food packaging materials remains relatively limited. Fotie and colleagues introduced the production of high gas barrier laminated films using concentrated CNCs coating dispersion obtained through sulfuric acid hydrolysis.[28,29] Conversely, our recent work involved a pullulan-based coating formulation reinforced with enzymatically derived BCNCs as organic nanofillers, applied to bare polyethylene terephthalate (PET) substrate to enhance its barrier performance.[30]

Remarkably, there are no existing works in the current literature that investigate the influence of acid type on hydrolysis degree and structural characteristics of BCNCs intended for integration into biopolymeric matrices to enhance their inherent barrier properties. Hence, this study addresses, for the first time, the development and application of a bionanocomposite coating formulation with low oxygen permeability attributes by utilizing acid-derived cellulose nanocrystals of bacterial origin (*K. sucrofermentans*). The primary polymer phase consists of the exopolysaccharide pullulan, known for its distinctive functional properties that make it suitable for various applications.[31] The plastic substrate chosen for the study is polyethylene terephthalate (PET), commonly used in the food packaging sector.

Prompted by an increasing interest in environmentally sustainable solutions, this study specifically aims to: (i) comprehensively investigate the impact of different disrupting acids (sulfuric, and hydrochloric) on the stability and morphological features of resulting BCNCs, and (ii) evaluate the gas barrier and optical/mechanical properties of pullulan/BCNCs coatings applied on a commonly used plastic (*i.e.*, PET), with the objective to acquire a preliminary information on the potential of this new coating for the creation of fully compostable packaging materials with high oxygen barrier performance.

2. Materials and methods

2.1. Production of macro-sized bacterial cellulose (BC)

BC was obtained through static fermentation (7 days at 30 °C) using *Komagataeibacter sucrofermentans DSM 15973* strain (Leibniz Institute DSMZ-German Collection of Microorganisms and Cell Cultures, Braunschweig Germany), and Hestrin and Schramm (HS) medium.[8] The resulting BC pellicles were removed from the medium, washed with deionized water, and boiled in a 1 M NaOH solution for 30 minutes to eliminate residual bacterial cells. After multiple washing cycles with distilled water, the cellulosic material was initially homogenized for 15 minutes using an ultra-turrax® T25 basic (Ika-Werke, Staufen, Germany), set at 12 000 rpm, and subsequently lyophilized (−55 °C, 0.63 mbar × 24 hours) with an ALPHA 1-2 LDplus freeze dryer (Martin Christ, Osterode am Harz, Germany).

2.2. Generation of bacterial cellulose nanocrystals (BCNCs)

The top-down process of converting bacterial cellulose into its nanocrystals was conducted using hydrochloric and sulfuric acid-driven hydrolysis.[32] Specifically, BCNCs were derived from a stock dispersion of BC, prepared by adding 12 g of freeze-dried BC to 88 mL of distilled water. Then, 1 g of the stock dispersion was mixed with 14 g of either 33 vol% reagent-grade hydrochloric acid (Merck KGaA, Darmstadt, Germany), or 65 vol% sulfuric acid (Sigma-Aldrich, Milan, Italy). To enhance acid penetration into the cellulosic structure, BC dispersions were mixed using an ultra-turrax at 8000 rpm for 5 minutes before undergoing the hydrolysis step.

Both chemical processes were carried out under magnetic stirring (400 rpm) at 60 ± 1 °C for 6 hours when using hydrochloric acid, resulting in H-BCNCs, or at 55 ± 1 °C for 2 hours when sulfuric acid was utilized to produce S-BCNCs.[34] The hydrolysis reaction was stopped by adding 14 mL of cold distilled water, followed by four cycles of centrifugation at 4000 rpm for 20 minutes each (Frontier™ 5000 Series Multi centrifuge, Ohaus, Parsippany, USA). After each separation cycle, bacterial cellulose nanocrystals were collected at the

bottom of the centrifuge tubes as pellets, with the acidic supernatant being discarded and replaced with fresh distilled water. The pellet was then redispersed through high-shear mixing (3000 rpm, 3 minutes). A further purification step was performed exclusively for sulfuric acid-derived BCNCs using a dialysis tube against deionized water (MW cut-off: 12 000 Da) (Sigma-Aldrich, Milan, Italy) until the effluent reached neutral pH values.

2.3. Bionanocomposite coating preparation

Pullulan powder (PI-20 grade, MW ≈ 200 kDa), purchased from Hayashibara Biochemical Laboratories Inc. (Okayama, Japan), was used as the main biopolymeric phase. Coating formation involved gently mixing of pullulan powder (10 wt%) and BCNCs (10 wt% wet basis, resulting in a dry nanocrystal content of 0.16 ± 0.01 wt% for H-BCNCs and 0.18 ± 0.01 wt% for S-BCNCs) at constant temperature (25 °C) under agitation (800 rpm) for up to 30 minutes.[30] The bio-nanocomposite dispersions were then applied to the corona-treated side of a polyethylene terephthalate (PET) film (12.0 ± 0.5 μm thick Arya-PET A410, JBF RAK LLC, Ras Al Khaimah, United Arab Emirates), kindly supplied by SAES Coated Films S.p.A. (Roncello, Italy). Specifically, about 3 mL of the nanocomposite dispersion was spread over a rectangular (24 × 18 cm^2) PET sample, securely positioned on an automatic film applicator (TQC Sheen Instruments, Capelle aan den IJssel, The Netherlands). The PET coating was performed in accordance with ASTM D823-07-Practice C, at a constant speed of 150 mm min^{-1}, using a horizontally placed steel rod with an engraved pattern, resulting in coatings of approximately equal nominal dry thickness of ≈ 1 μm. Following water evaporation, accomplished through a steady and perpendicular flow of mild air (25.0 ± 0.5 °C for 3 minutes) at a distance of 40 cm from the applicator,[33,34] the coated samples were stored under controlled conditions (23 °C, 0% relative humidity (RH)) until their characterization.

For comparison purposes, PET films coated solely with pullulan were also subjected to analysis throughout the experimental study.

2.4. Analyses

2.4.1. Characterization of BCNCs dispersion. The yield of the hydrolytic processes was determined gravimetrically using a halogen-lamp moisture content analyzer HS43S-MC (Mettler Toledo, Greifensee, Switzerland), set at 105 °C.[32] The stability of both nanostructured water-based dispersions was monitored over a time span of 25 days through turbidimetric analysis using a Lambda 25 spectrophotometer (PerkinElmer, Waltham, USA). BCNCs aqueous dispersions (0.1 wt%) were subjected to transmittance mode scanning across a broad wavelength range (λ = 380–800 nm), and the area under each resulting spectrum was then determined using the PerkinElmerUV WinLab software, version 6.0.4.0738. This parameter, inversely correlated with sample turbidity influenced by nanocrystals aggregation, was used as an indicator of sample stability over time.

ζ-Potential was evaluated through electrophoretic light scattering (ELS) using a LitesizerTM 500 (Anton Paar, Rivoli, Italy) system at neutral pH.

Size distribution measurements were conducted using photon correlation spectroscopy experiments *via* a dynamic light scattering (DLS) Nanotrac Flex *In situ* Analyzer (MicroTrac GmbH, Krefeld, Germany). Tests were carried out at 25 °C with a stabilization time of 60 seconds, using water properties (viscosity = 0.8872 cP, refractive index = 1.33) as the reference. The software employed the non-negative least squares algorithm for size distribution calculation. The scattering radiation of BCNCs water dispersion (0.1 wt%) was assessed through haze analysis using a Lambda 650 spectrophotometer (PerkinElmer, Waltham, USA), coupled with a 150 mm diameter integrative sphere to capture the diffused light (λ = 380–780 nm) from the sample. The calculation of diffracted radiation was:

$$\text{Haze (\%)} : \left\{\left(\frac{T4}{T2}\right) - \left(\frac{T3}{T1}\right)\right\} \times 100 \quad (1)$$

where $T1$ represents the incident radiation, $T2$ is the overall sample transmittance, $T3$ is the radiation emitted by the instrument, and $T4$ denotes radiation emitted by both the instrument and the sample.

Transmission electron microscopy (TEM) images of BCNCs were captured using an LEO 912 AB energy-filtering transmission electron microscope (EF-TEM) (Carl Zeiss, Oberkochen, Germany), operating at 80 kV. Digital images were taken using a ProScan 1K Slow-Scan CCD camera (Proscan, Scheuring, Germany). Samples for TEM analysis were prepared by drop-casting a few mL of BCNCs dispersion onto Formvar-coated Cu grids (400-mesh) and allowing them to rest for 24 hours at room temperature for water evaporation.

Qualitative visualization of self-organization phenomena in aqueous BCNCs dispersions (0.1 wt%) was achieved through the appearance of a characteristic fingerprint, such as iridescent birefringence. Due to the absence of any charge on the hydrochloric acid-derived BCNCs backbone, the stacked nanocrystals were dispersed by dissolving 0.5 wt% pullulan powder in aqueous H-BCNCs, followed by ultrasonication using a UP400S (400 W, 24 kHz) ultrasonic device (Hielscher, Teltow, Germany) under the following conditions: 0.3 s s^{-1} cycle, 30% amplitude, and 1 minute treatment duration. This approach enabled pullulan biopolymer dissolved in H-BCNCs aqueous dispersions to act as a 'spacer' between the stacked nanocrystals after ultrasonication. The transition from the isotropic phase (randomly oriented BCNCs) to the anisotropic phase (unidirectionally self-oriented BCNCs) was observed using magnetic stirring (200 rpm) and cross-polarized light regardless of the sample under investigation.[17]

2.4.2. Characterization of PET/bio-nanocomposite coated films. The optical properties of both bare and coated PET films were evaluated in terms of haze (in %), a measure that detects surface irregularities or bulk defects by quantifying the light scattered by the sample. Notably, haze is related to the material's "see-through" capability, which refers to its ability to clearly display items (*e.g.*, food products) positioned behind it.[33]

Similarly to the approach described in the previous paragraph, analyses were conducted according to ASTM D 1003-00 using a Lambda 650 spectrophotometer coupled with an integrative sphere (λ = 380–780 nm).

To gain further insight into the morphological characteristics of the investigated films, atomic force microscopy (AFM) experiments were carried out using a Nanoscope V Multimode (Bruker, Karlsruhe, Germany) in intermittent-contact mode. For the analysis, 10 μL of a 1 : 10 diluted BCNCs dispersion were dropped onto a mica substrate (Ted Pella Inc., Redding, California). Images were captured at a resolution of 512 × 512 pixels using silicon tips (force constant: 3 N m^{-1}; resonance frequency: ~75 kHz). Dimensional calculations and image editing were performed using Nanoscope software (version 7.30; Bruker, Karlsruhe, Germany).

Cross-sections and surface topography of both uncoated and coated PET films were examined using a Leo 1430 scanning electron microscope (SEM) (Zeiss, Oberkochen, Germany) to gather data on the overall thickness following final coating deposition. Surface test specimens were mounted on metallic stubs covered with carbon tape, while cross-sectioned samples were thinly sliced with a scalpel and mounted on a thin specimen split-mount holder. Prior to microscopy, the samples were sputter-coated with gold to an approximate thickness of 10 nm using an Agar High-Resolution Sputter Coater (model 208RH).

Mechanical parameters of coated and uncoated films were evaluated using a Z005 dynamometer (Zwick Roell, Ulm, Germany) coupled to the software TestXpertV10.11 Master for data elaboration. More specifically, the bonding strength (BS, in N/15 mm) between coating and PET was measured *via* a T-peel test following the AIMCAL (Association of Industrial Metallizers, Coaters and Laminators) TP-104-87 procedure. Elastic modulus (E, in GPa), elongation at break (ε_B, in %), and tensile strength (TS, in MPa), were obtained by a tensile test according to ASTM D882. Tests were carried out on film strips 15 cm in length and 2.54 cm in width employing a 5 kN load cell connected with two clamps 10 cm apart.

The oxygen barrier properties of bare PET films, pullulan-coated PET films, and BCNCs/pullulan-coated PET films were evaluated using a MultiPerm permeability analyzer (Permtech Srl, Lucca, Italy), equipped with an electrochemical sensor. This instrument employs the isostatic method, which establishes equal total pressure on both sides of the specimen (*i.e.*, the film). A 50 cm^2 sample surface is placed between two semi-chambers through which an inert gas (usually nitrogen) continuously flows. After initial conditioning, the test gas (oxygen) is introduced, permeates the sample, and is transported to the detector by the inert gas. The partial pressure of the test gas remains constant (1 atm) during the analysis to ensure a consistent driving force. Oxygen transmission rate (OTR, $cm^3\ m^{-2}\ 24\ h^{-1}$) values were determined following the ASTM F2622-08 standard method, with a carrier flow (N_2) of 10 mL min^{-1} at 23 °C, under two different relative humidity (RH) levels: 0% and 80%. Analyses were performed with the coated side of each sample facing the upper semi-chamber into which humid test gas (oxygen) was introduced.[30]

2.5. Statistical analysis

All experiments and analyses were performed at least in triplicate. Data were analyzed using Statgraphics Plus 4.0 software (STSC, Rockville, MD, USA), with a one-way analysis of variance (ANOVA) and Tukey test being used to check for significant differences among samples. The significance level (p) was fixed at 0.05.

3. Results and discussion

3.1. Hydrolysis yield and stability of BCNCs dispersions

The yield of cellulose fragmentation mediated by hydrochloric and sulfuric acid was found to be 69.83 ± 3.94% DW and 51.61 ± 1.51% DW, respectively. The significant ($p < 0.05$) difference observed between these mean values can be attributed to the slightly higher concentration of sulfuric acid applied, resulting in a more severe attack on the cellulosic backbone. In a similar vein, Vasconcelos *et al.* (2017)[35] proposed that the more pronounced surface erosion of BC when sulfuric acid was used, as compared to the erosion achieved with HCl, was likely due to partial hydrolysis of the cellulose crystalline region.

Turbidity experiments were conducted to monitor the stability evolution of BCNCs dispersions over 25 days. The collected results are depicted in Fig. 1 for both investigated acids. As observed, reasonable stability was exhibited by H-BCNCs samples up to 7 days of storage, after which a sharp decrease in transmittance values occurred. Conversely, S-BCNCs demonstrated a more consistent stability throughout the entire time window. This trend can be explained by the presence of $-SO_4^{2-}$ groups along the S-BCNCs backbone at the C-6 position of the glucose molecule, which likely induced strong intermolecular repulsion forces, thus hindering aggregation. However, the transmittance of the S-BCNCs dispersion slightly decreased (*i.e.*, turbidity increased) mainly because not all hydroxyl groups at the C-6 position of the glucose molecule were esterified with $-SO_4^{2-}$ groups. Therefore, a potential breakdown in repulsion among negatively charged sulfate half-ester BCNCs could have occurred, considering they were present at a ratio of one in every 18th glucose unit before desulfation.[36] Hydrochloric acid led to the formation of uncharged nanocrystals (*i.e.*, rich in –OH groups), which prompted nearly immediate aggregation of BCNCs. This process led to the formation of new hydrogen bonds among nanocrystals, replacing the initial bonds and resulting in reduced transmittance values (*i.e.*, increased turbidity) due to BCNCs stacking.

The results from Fig. 1 were further corroborated by ζ-potential measurements. Specifically, ζ-potential values of −33.01 ± 0.2 mV for S-BCNCs, and −15.50 ± 0.2 mV for H-BCNCs aqueous dispersions were obtained, respectively. According to a study by Clogston & Patri (2011),[37] ζ-potential values exceeding |30| mV are desirable to maintain stable colloidal dispersions. As mentioned earlier, the modification of the cellulosic backbone induced by sulfuric acid-mediated hydrolysis, resulting in the esterification of hydroxyl groups at the C-6 position to form sulfate groups, contributed to the

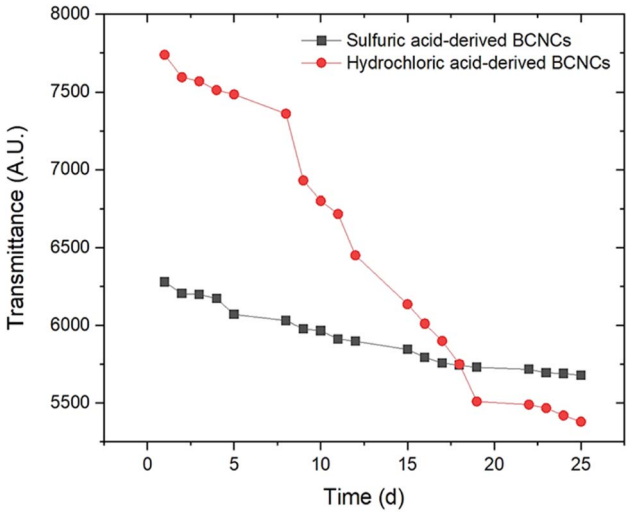

Fig. 1 Evolution of H-BCNCs and S-BCNCs dispersion stability (expressed as the area beneath each transmittance spectrum) over the course of 25-days time frame.

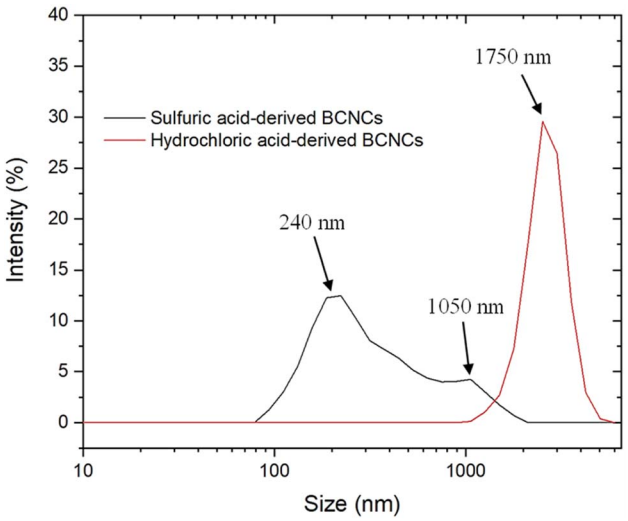

Fig. 3 Size distribution intensity curves, acquired through dynamic light scattering (DLS) measurements, for nanocrystal dispersions resulting from both hydrochloric acid- and sulfuric acid-hydrolyzed BC.

improved stability of S-BCNCs dispersions. Conversely, ζ-potential values below |30| mV produce less stable colloidal dispersions, which are prone to aggregation, flocculation, and phase separation over time. Specifically for H-BCNCs, initial aggregation of newly formed –OH-rich nanocrystals occurred spontaneously.

3.2. Morphological properties of BCNCs dispersions

Cellulose chains are arranged in elementary fibrils, which are in turn organized into both highly ordered (*e.g.*, crystalline) structure zones, and amorphous-like (*e.g.*, disordered) regions. Crystalline domains are known as CNCs, the differences in length and width of which seems to depend on the applied miniaturization process rather than to the originating source of cellulose (*e.g.*, agro-wastes, bacteria).[38]

Irrespective of the hydrolyzing agent used, BCNCs obtained in this work had a straight needle-like morphology, as clearly visible from the TEM images in Fig. 2. The cellulosic breakage induced by HCl treatment resulted in a heterogeneous nano-to-micro magnitude dispersion of rod-like nanocrystals, with a length varying from ~800 nm to ~2.5 μm, and an average width of about 30 nm. These findings agree with those emphasized in the work of Liu *et al.* (2015),[39] where an average BCNCs length of 2–3 μm was reported. Notably, the –OH-rich nanocrystals dispersed in distilled water tended to aggregate in stacks of 3 to 10 piled whiskers due to extensive hydrogen bonding (Fig. 2a). This phenomenon aligns with the previously observed decrease in dispersion transmittance over time (Fig. 1). In contrast, the dimensional range displayed by S-BCNCs was considerably smaller, with the length of the

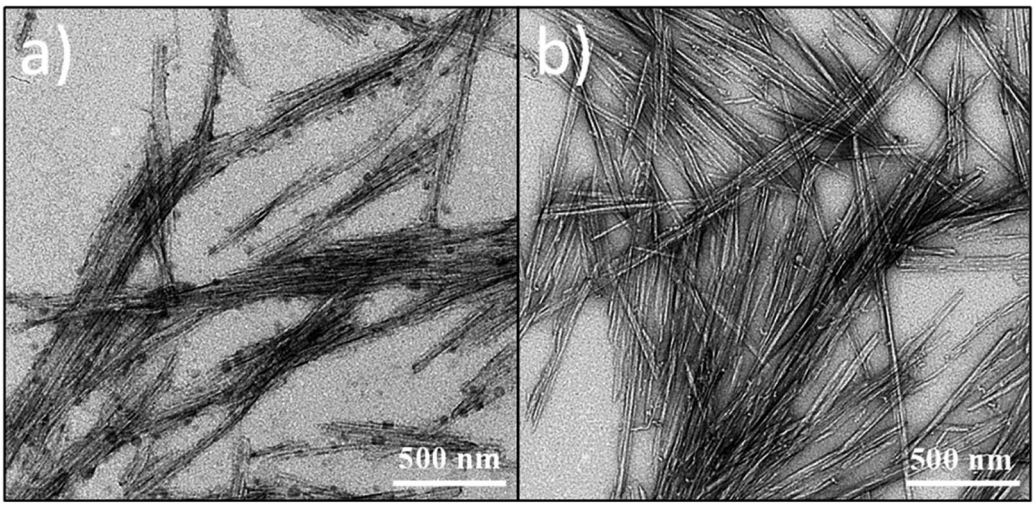

Fig. 2 Transmission electron microscopy (TEM) images of needle-like BCNCs obtained after HCl (a) or H_2SO_4 (b) hydrolysis of BC.

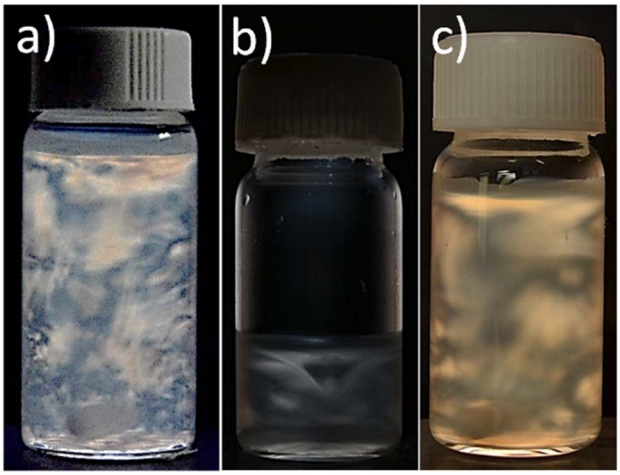

Fig. 4 Unidirectional self-orientation of rod-like BCNCs into a nematic liquid crystalline alignment (*i.e.*, anisotropic phase) using cross-polarized light. The iridescent birefringence of sulfuric acid-derived and pullulan/hydrochloric acid-based BCNCs is shown in panel a and panel c, respectively. The panel b shows the lack of chiral nematic order in uncharged H-BCNCs.

needle-like nanocrystals ranging between ~200 nm and ~570 nm, along with a reduced width (≈22 nm). The spatial arrangement of S-BCNCs, characterized by individual whisker structures rather than stacked piles, seems to support the theory suggesting substantial repulsion forces among $-SO_4^{2-}$ rich units (Fig. 2b).

The most significant extent of cellulosic backbone cleavage upon sulfuric acid treatment was confirmed by the results of DLS measurements (Fig. 3). Despite its inadequacy in determining the absolute size distribution of non-spherical particles,[8] we opted to perform DLS experiments solely to assess any emerging differences in the size of H-BCNCs and S-BCNCs. As depicted in Fig. 3, H-BCNCs presented a single and sharp peak between 1.5 μm and 2.1 μm in size. In contrast, S-BCNCs exhibited a bimodal size distribution, with a more prominent peak centered at ~240 nm and a smaller one at around 1 μm. The presence of the second dimensional group in S-BCNCs could be attributed to an incomplete top-down process after 2 hours of acid hydrolysis, which might have left a reasonable amount of larger micro-scale particles in the dispersion.

3.3. Optical properties of BCNCs dispersions

Theoretically, a decrease in size down to the nanoscale level reduces scattering effects from nanoparticles, as the amplitude of the incident light becomes greater than or equal to the nanoparticles' dimensions. In line with the results presented in Fig. 1 and 3, it was observed that the percentage of light scattered from larger H-BCNCs whiskers (75.81 ± 5.16%) was significantly ($p < 0.05$) higher than that generated by the smaller S-BCNCs particles (59.76 ± 6.53%). Similar conclusions were drawn by Preston *et al.* (2013)[40] in their investigation of the optical characteristics of conductive silver nanowire films.

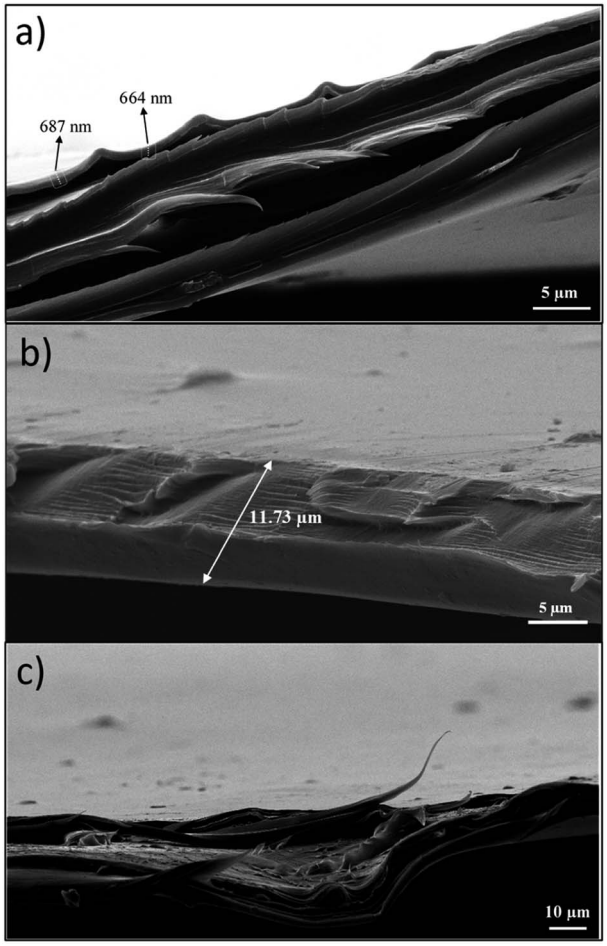

Fig. 5 Scanning electron microscopy (SEM) micrographs of the bio-nanocomposite PET coated films: (a) thickness of the coating layer; (b) thickness of the overall PET coated film; (c) surface features of the coated films.

The negatively charged S-BCNCs whiskers disperse uniformly in water through electrostatic repulsions provided by sulfate groups. Consequently, the homogeneously concentrated S-BCNCs system spontaneously arranges into impressive liquid crystalline formations. Specifically, with an increase in nanocrystal concentration, a nematic liquid crystalline alignment (*i.e.*, an anisotropic phase) is adopted, characterized by a unidirectional self-orientation of the rod-like BCNCs. These chiral nematic or cholesteric structures in the anisotropic phase consist of stacked planes of nanocrystal rods aligned along a vector (director), with the orientation of each director rotating on a perpendicular axis from one plane to the next. The induced parallel alignment of BCNCs is attributed to the well-known entropically driven self-orientation phenomenon of rod-like species to achieve nematic order.[17] This characteristic behavior is clearly demonstrated in Fig. 4a, where iridescent birefringence (*i.e.*, anisotropic crystalline arrangements) of S-BCNCs was observed after magnetic stirring. Conversely, the uncharged H-BCNCs did not exhibit the same phenomenon (Fig. 4b), underscoring the vital role of the negatively charged sulfate groups, located on the BCNCs' surface, in promoting phase stability. Nevertheless, to prevent H-BCNCs

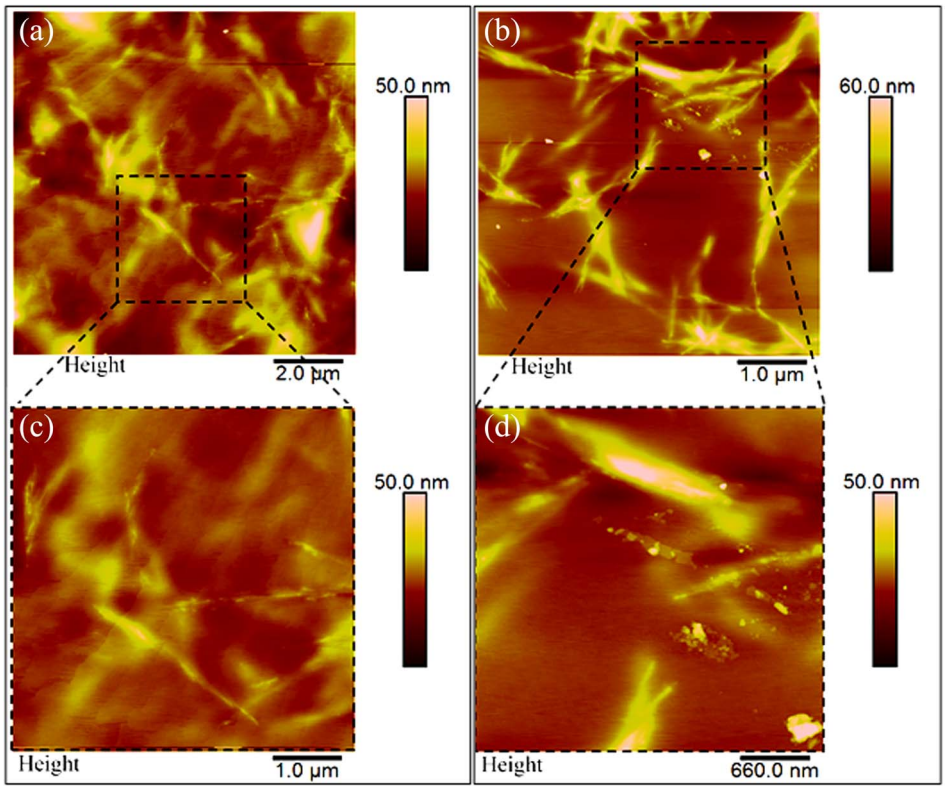

Fig. 6 Atomic force microscopy (AFM) height images of PET/bio-nanocomposite films coated with H-BCNCs (a) and S-BCNCs (b). Zoomed-in areas are presented below the main panels (c and d).

stacking, the uncharged system was supplemented with 0.5 wt% pullulan powder (see Materials and methods section). At this stage, nanocrystals were sterically stabilized through surfactant coating or polymer grafting,[17,41,42] leading to twists in the nanocrystal structure and thereby enhancing birefringence (Fig. 4c). Specifically, pullulan facilitated the unidirectional self-orientation of the rod-like BCNCs by acting as an organic spacer among the uncharged nanocrystals. Consequently, the self-organization into a nematic liquid crystalline alignment (*i.e.*, an anisotropic phase) of pullulan-loaded H-BCNCs dispersions was observed.

3.4. Morphological properties of PET/bionanocomposite coated films

Scanning electron microscopy (SEM) and atomic force microscopy (AFM) analyses were conducted to measure the thickness of the pullulan/BCNCs-based coating and to explore both the topography and morphological features of the resulting bio-nanocomposite PET-coated films. The thickness of the deposited coating layer on the PET substrate was approximately 0.7 μm, slightly deviating from the expected nominal value of 1 μm (Fig. 5a). According to previous research,[33] this observed discrepancy can likely be attributed to an uneven deposition of the bionanocomposite coating layer, possibly due to the saturation of the wire-wound rod. Additionally, the inherent variability in the corona-treatment efficiency of bare PET might have impacted the accurate deposition of the coating layer. However, the overall thickness of the bio-nanocomposite film was macroscopically maintained as compared to the original bare PET sheet (Fig. 5b). Given that the bare PET surface exhibits significant surface roughness,[43] the smoothening effect resulting from the coating deposition on the plastic substrate was evident (Fig. 5c), owing to the ability of pullulan/BCNCs to fill the inherent irregularities on the PET surface.

Table 1 Haze, tensile parameters, and oxygen transmission rate (OTR) of uncoated, pullulan-coated, and pullulan/BCNCs-coated PET films. Different superscript letters within the same column indicate statistical differences among samples ($p < 0.05$)

		Tensile parameters			OTR ($cm^3\ m^{-2}\ 24\ h^{-1}$)	
PET sample	Haze (%)	E (GPa)	ε_B (%)	TS (MPa)	23 °C–0% RH	23 °C–80% RH
Pristine (uncoated)	2.3 ± 0.1^a	2.67 ± 0.44^a	25.1 ± 6.1^a	135.1 ± 11.1^a	121.8 ± 1.8^a	110.1 ± 1.2^a
Pullulan coated	2.1 ± 0.2^a	2.58 ± 0.57^a	28.3 ± 8.4^a	125.1 ± 8.2^a	6.3 ± 0.2^b	102.1 ± 2.5^b
Pullulan/H-BCNCs coated	2.0 ± 0.1^a	2.61 ± 0.44^a	24.9 ± 6.7^a	131.7 ± 10.9^a	2.6 ± 0.3^c	94.8 ± 2.1^b
Pullulan/S-BCNCs coated	2.0 ± 0.1^a	2.62 ± 0.53^a	24.3 ± 8.9^a	128.4 ± 15.8^a	1.8 ± 0.4^c	87.2 ± 2.7^c

Table 2 Haze and oxygen transmission rate (OTR) at 0% relative humidity (RH) for biopolymer-coated PET samples, both found in this study and retrieved from recent literature findings[a]

Coating agent	Haze (%)	OTR (cm^3 m^{-2} 24 h^{-1}) 23 °C–0% RH	Ref.
Nanocomposite: pullulan + BCNCs	2.0–2.1	1.80–6.30	This work
Nanocomposite: pullulan + BCNCs	N.R.	0.70–6.20	30
Nanocomposite: pullulan + graphene oxide	2.5–3.3	0.01–0.99	33
Nanostructure: pullulan + silica	N.R.	0.96–82.30	46
Nanocomposite: pullulan + mica	2.7–3.2	0.01–1.27	49
Cellulose nanofibers (CNF) + chitin nanowhiskers (ChNW)	1.7–2.5	0.51–0.97	50
CNF + ChNW	N.R.	1.60–27.00	51
CNCs	1.9	≈2.00	52
CNCs	N.R.	0.38–4.82	53
CNCs	3.3	≈2.00	54

[a] N.R. = not reported.

Further examination of the surface features of the H-BCNCs and S-BCNCs loaded pullulan coatings was carried out through AFM analysis (Fig. 6). Remarkably, regardless of the specific sample, a single-whisker-like morphology was observed, with constituent particles having a length of 0.5 to 3 μm, and a width of 5 to 55 nm, in complete agreement with the results of TEM observations (Fig. 2). This underscores the crucial role of pullulan in effectively dispersing individual nanocrystals, thus preventing their aggregation especially in the case of S-BCNCs (Fig. 6b) in the final nanostructured formulation and thereby preserving their inherent functionality.

3.5. Optical, mechanical, and oxygen barrier properties of PET/bionanocomposite coated films

Table 1 presents the haze, tensile parameters, and OTR values of pristine PET, pullulan-coated PET, and bionanocomposite-coated PET based on H-BCNCs and S-BCNCs. The application of the coating on the plastic substrate did not impair its original optical and tensile properties, as indicated by the lack of statistically significant ($p > 0.05$) differences among mean values, regardless of the material used for the coating formulation. In particular, considering that haze values within the 3.0% threshold are necessary to ensure suitable visibility of items behind a plastic film,[44] the developed coatings are undoubtedly appropriate for packaging applications that require high transparency characteristics.

Remarkable outcomes were also obtained from OTR measurements, where the sole pullulan coating resulted in a 20-fold increase in oxygen barrier properties for the pristine PET film (Table 1). The inclusion of BCNCs within the main biopolymeric phase furtherly improved the oxygen barrier performance of the final material. Besides the inherent oxygen barrier properties of both pullulan and BCNCs, the excellent performance of the coating under dry conditions can also be attributed to the excellent bonding strength between coating and substrate (5.1 ± 0.5 N/15 mm). Despite the superior barrier properties displayed by the S-BCNCs/pullulan bionanocomposite-coated film, we refrained from speculating on the superior material due to the lack of statistical differences ($p > 0.05$) with the H-BCNCs counterpart. In line with recent findings,[30,33] the inferred protection against oxygen permeation is attributed to the interface effects of 1D nanoparticles (such as cellulose nanocrystals), rather than an increase in the tortuous path characteristic of 2D nanocomposite systems (like graphene and montmorillonite platelets). Noteworthy, the water vapor transmission rate (WVTR) of the uncoated PET (~15.5 g m^{-2} 24 h^{-1} at 38 °C/90% RH) did not appreciably change neither after the deposition of pullulan alone nor when combined with H-BCNCs or S-BCNCs (data not shown). This demonstrates that the coating cannot act as a barrier against water vapor.

Based on the demonstrated OTR performance, the bionanocomposite/PET system developed in this study could serve as a viable alternative to various commercially available solutions, including PET coated with ethylene(vinyl alcohol), poly(vinyl alcohol), and polyvinylidene chloride, particularly when low humidity levels are necessary for food storage and preservation.[45] However, an opposite behavior was observed in humid environments (80% RH). Specifically, due to the water-sensitive nature of the bionanocomposite coating formulation, OTR values for the bare PET film were nearly restored (Table 1). These results are supported by previous scientific research,[46–48] and ascribed to water molecules competing for the –OH groups displaced along both the biopolymer and filler backbones and participating in intermolecular hydrogen bonding.[30,33]

Overall, our data are in line with the results obtained in other works (Table 2), demonstrating the potential of biopolymer coatings to improve the oxygen barrier properties of PET without jeopardizing its intrinsic optical properties.

4. Conclusions

The hydrolysis of bacterial cellulose using hydrochloric and sulfuric acids yielded high reaction yields and a rod-like nanocrystal morphology, as evidenced by gravimetric, TEM, and AFM analyses. The stability of the nanocrystals' aqueous dispersion and the presence of the iridescent birefringence were more pronounced in the case of S-BCNCs as compared to H-BCNCs.

This difference could be attributed to the esterification of hydroxyl groups at the C-6 position to form sulfate groups in S-BCNCs, which might have promoted interparticle repulsion.

Pullulan served as the primary polymer phase in the generation of BCNCs bionanocomposite coatings, aimed at creating a high oxygen barrier layer when applied to a PET film. BCNCs-reinforced pullulan coating displayed the most favorable results in terms of haze and oxygen barrier properties. However, these oxygen barrier properties were completely compromised on bare PET film when RH was raised to 80%.

In conclusion, the characteristics of the final coated packaging film suggest its suitability for specific food applications, such as dry products, while also highlighting its inherent limitations for the preservation of moist and high-water activity foods. The use of raw materials of renewable origin (cellulose and pullulan) can pave the way to new packaging configurations with enhanced performance, such as bionanocomposite coatings applied to compostable plastics (*e.g.*, PLA) or fully cellulosic materials (*e.g.*, paper pouches).

Author contributions

Daniele Carullo & Cesare Rovera: conceptualization, data curation, formal analysis, investigation, methodology, writing – original draft. Tommaso Bellesia: formal analysis. Duygu Büyüktaş & Masoud Ghaani: writing – review & editing. Nadia Santo & Diego Romano: methodology, writing – review & editing. Stefano Farris: conceptualization, methodology, funding acquisition, supervision, project administration, writing – review & editing.

Conflicts of interest

There are no conflicts to declare.

Acknowledgements

This study was carried out within the Agritech National Research Center and received funding from the European Union Next-GenerationEU (PIANO NAZIONALE DI RIPRESA E RESILIENZA (PNRR) – MISSIONE 4 COMPONENTE 2, INVESTIMENTO 1.4 – D. D. 1032 17/06/2022, CN00000022). This manuscript reflects only the authors' views and opinions, neither the European Union nor the European Commission can be considered responsible for them.

References

1 V. Giovenzana, A. Casson, R. Beghi, A. Tugnolo, S. Grassi, C. Alamprese, E. Casiraghi, S. Farris, I. Fiorindo and R. Guidetti, *Chemical Engineering Transaction*, 2019, **75**, 193–198.
2 P. P. Das, P. Kalyani, R. Kumar and M. Khandelwal, *Sustainable Food Technology*, 2023, **1**, 528.
3 H. Bian, Y. Gao, J. Luo, L. Jiao, W. Wu, G. Fang and H. Dai, *Waste Manage.*, 2019, **91**, 1–8.
4 T. Y. Chong, M. C. Law and Y. S. Chan, *J. Polym. Environ.*, 2021, **29**, 363–381.
5 S. Ventura-Cruz and A. Tecante, *Food Hydrocolloids*, 2021, **118**, 106771.
6 M. Gullo, S. La China, P. M. Falcone and P. Giudici, *Appl. Microbiol. Biotechnol.*, 2018, **102**, 6885–6898.
7 K. Tajima, T. Imai, T. Yui, M. Yao and I. Saxena, *Cellulose*, 2022, **29**, 2755–2777.
8 C. Rovera, M. Ghaani, N. Santo, S. Trabattoni, R. T. Olsson, D. Romano and S. Farris, *ACS Sustain. Chem. Eng.*, 2018, **6**, 7725–7734.
9 J. Yao, S. Chen, Y. Chen, B. Wang, Q. Pei and H. Wang, *ACS Appl. Mater. Interfaces*, 2017, **9**, 20330–20339.
10 A. Kirui, Z. Ling, X. Kang, M. C. Dickwella Widanage, F. Mentink-Vigier, A. D. French and T. Wang, *Cellulose*, 2019, **26**, 329–339.
11 D. Andriani, A. Y. Apriyana and M. Karina, *Cellulose*, 2020, **27**, 6747–6766.
12 D. A. Gregory, L. Tripathi, A. T. Fricker, E. Asare, I. Orlando, V. Raghavendran and I. Roy, *Mater. Sci. Eng., R*, 2021, **145**, 100623.
13 P. Cazón, G. Velázquez and M. Vázquez, *Carbohydr. Polym.*, 2019, **216**, 72–85.
14 P. Cazón and M. Vázquez, *Food Hydrocolloids*, 2021, **113**, 106530.
15 M. S. Andrade, O. H. Ishikawa, R. S. Costa, M. V. S. Seixas, R. C. L. B. Rodrigues and E. A. B. Moura, *Food Packag. Shelf Life*, 2022, **31**, 100807.
16 S. M. El-Sayed and A. M. Youssef, *Sustainable Food Technology*, 2023, **1**, 215.
17 Y. Habibi, L. A. Lucia and O. J. Rojas, *Chem. Rev.*, 2010, **110**, 3479–3500.
18 E. Y. Wardhono, H. Wahyudi, S. Agustina, F. Oudet, M. P. Pinem, D. Clausse, K. Saleh and E. Guénin, *Nanomaterials*, 2018, **8**, 859.
19 D. K. Arserim-Uçar, F. Korel, L. Liu and K. L. Yam, *Food Chem.*, 2021, **336**, 127597.
20 S.-A. Park, Y. Eom, H. Jeon, J. M. Koo, E. S. Lee, J. Jegal, S. Y. Hwang, D. X. Oh and J. Park, *Green Chem.*, 2019, **21**, 5212–5221.
21 H. M. C. Azeredoa, M. F. Rosa and L. C. Mattoso, *Ind. Crops Prod.*, 2017, **97**, 664–671.
22 I. Gan and W. S. Chow, *Food Packaging and Shelf Life*, 2018, **17**, 150–161.
23 F. Luzi, E. Fortunati, A. Jiménez, D. Puglia, D. Pezzolla, G. Gigliotti, J. M. Kennya, A. Chiralt and L. Torre, *Ind. Crops Prod.*, 2016, **93**, 276–289.
24 E. Fortunati, M. Gigli, F. Luzi, F. Dominici, N. Lotti, M. Gazzano, A. Cano, A. Chiralt, A. Munari, J. M. Kenny, I. Armentano and L. Torre, *Carbohydr. Polym.*, 2017, **165**, 51–60.
25 L. N. Ludueña, E. Fortunati, J. I. Morán, V. A. Alvarez, V. P. Cyras, D. Puglia, L. B. Manfredi and M. Pracella, *J. Appl. Polym. Sci.*, 2016, **133**, 43302–43311.
26 S. T. Gedarawatte, J. T. Ravensdale, H. Al-Salami, G. A. Dykes and R. Coorey, *Carbohydr. Polym.*, 2021, **251**, 117096.

27 M. Salari, M. S. Khiabani, R. R. Mokarram, B. Ghanbarzadeh and H. S. Kafil, *Food Hydrocolloids*, 2018, **84**, 414–423.
28 G. Fotie, L. Amoroso, S. Limbo, G. Muratore and L. Piergiovanni, *Ital. J. Food Sci.*, 2019, 8–14.
29 G. Fotie, S. Gazzotti, M. A. Ortenzi and L. Piergiovanni, *Appl. Sci.*, 2020, **10**, 3201.
30 C. Rovera, F. Fiori, S. Trabattoni, D. Romano and S. Farris, *Nanomaterials*, 2020, **10**, 735.
31 S. Farris, I. U. Unalan, L. Introzzi, J. M. Fuentes-Alventosa and C. A. Cozzolino, *J. Appl. Polym. Sci.*, 2014, **131**, 40539–40550.
32 C. Rovera, D. Carullo, T. Bellesia, D. Duygu Büyüktaş, M. Ghaani, E. Caneva and S. Farris, *Front. Sustain. Food Syst.*, 2023, **6**, 1087867.
33 I. U. Unalan, D. Boyacı, M. Ghaani, S. Trabattoni and S. Farris, *Nanomaterials*, 2016, **6**, 244–254.
34 M. Rollini, A. Musatti, D. Cavicchioli, D. Bussini, S. Farris, C. Rovera, D. Romano, S. De Benedetti and A. Barbiroli, *Sci. Rep.*, 2020, **10**, 21358.
35 N. F. Vasconcelos, J. P. Feitosa, F. M. da Gama, J. Morais, F. K. Andrade, M. S. de Souza Filho and M. F. Rosa, *Carbohydr. Polym.*, 2017, **155**, 425–431.
36 S. Llàcer Navarro, K. Nakayama, A. Idström, L. Evenäs, A. Ström and T. Nypelö, *Cellulose*, 2021, **28**, 9633–9644.
37 J. D. Clogston and A. K. Patri, *Methods Mol. Biol.*, 2011, **697**, 63–70.
38 W. Tian, X. Gao, J. Zhang, J. Yu and J. Zhang, *Carbohydr. Polym.*, 2022, **277**, 118863.
39 D. Liu, Q. Wu, R. L. Andersson, M. S. Hedenqvist, S. Farris and R. T. Olsson, *J. Mater. Chem. A*, 2015, **3**, 15745.
40 C. Preston, Y. Xu, X. Han, J. N. Munday and L. Hu, *Nano Res.*, 2013, **6**, 461–468.
41 J. Araki and S. Kuga, *Langmuir*, 2001, **17**, 4493–4496.
42 L. Heux, G. Chauve and C. Bonini, *Langmuir*, 2020, **16**, 8210–8212.
43 F. Pilati, M. Montecchi, P. Fabbri, A. Synytska, M. Messori, M. Toselli, K. Grundke and D. Pospiech, *J. Colloid Interface Sci.*, 2007, **315**, 210–222.
44 L. Introzzi, T. O. Blomfeldt, S. Trabattoni, S. Tavazzi, N. Santo, A. Schiraldi, L. Piergiovanni and S. Farris, *Langmuir*, 2012, **28**, 11206–11214.
45 C. Rovera, M. Ghaani and S. Farris, *Trends Food Sci. Technol.*, 2020, **97**, 210–220.
46 S. Farris, L. Introzzi, J. M. Fuentes-Alventosa, N. Santo, R. Rocca and L. Piergiovanni, *J. Agric. Food Chem.*, 2012, **60**, 782–790.
47 C. A. Cozzolino, G. Cerri, A. Brundu and S. Farris, *Cellulose*, 2014, **21**, 4323–4335.
48 R. Rampazzo, D. Alkan, S. Gazzotti, M. A. Ortenzi, G. Piva and L. Piergiovanni, *Packag. Technol. Sci.*, 2017, **30**, 645–661.
49 I. U. Unalan, D. Boyacı, S. Trabattoni, S. Tavazzi and S. Farris, *Nanomaterials*, 2017, **7**, 281.
50 T. Kim, T. H. Tran, S. Y. Hwang, J. Park, D. X. Oh and B.-S. Kim, *ACS Nano*, 2019, **13**, 3796–3805.
51 V. T. T. Thuy, L. T. Hao, H. Jeon, J. M. Koo, J. Park, E. S. Lee, S. Y. Hwang, S. Choi, J. Park and D. X. Oh, *RSC Green Chemistry*, 2021, **23**, 2658–2667.
52 G. Fotie, R. Rampazzo, M. A. Ortenzi, S. Checchia, D. Fessas and L. Piergiovanni, *Polymers*, 2017, **9**, 415.
53 G. Fotie, L. Amoroso, G. Muratore and L. Piergiovanni, *Food Packag. Shelf Life*, 2018, **18**, 62–70.
54 F. Li, P. Biagioni, M. Bollani, A. Maccagnan and L. Piergiovanni, *Cellulose*, 2013, **20**, 2491–2504.